Defence Technology 33 (2024) 327–338

Contents lists available at ScienceDirect

Defence Technology

journal homepage: www.keaipublishing.com/en/journals/defence-technology

Hybrid pedestrian positioning system using wearable inertial sensors and ultrasonic ranging

Lin Qi [a], Yu Liu [a], Chuanshun Gao [b], Tao Feng [a], Yue Yu [a, *]

[a] School of Communication and Information Engineering, Chongqing University of Posts and Telecommunications, Chongqing 400065, China
[b] Department of Land Surveying and Geo-Informatics, The Hong Kong Polytechnic University, Hong Kong 999077, China

ARTICLE INFO

Article history:
Received 12 April 2023
Received in revised form
13 July 2023
Accepted 1 November 2023
Available online 7 November 2023

Keywords:
Pedestrian positioning system
Wearable inertial sensors
Ultrasonic ranging
Deep-learning
Data and model dual-driven

ABSTRACT

Pedestrian positioning system (PPS) using wearable inertial sensors has wide applications towards various emerging fields such as smart healthcare, emergency rescue, soldier positioning, etc. The performance of traditional PPS is limited by the cumulative error of inertial sensors, complex motion modes of pedestrians, and the low robustness of the multi-sensor collaboration structure. This paper presents a hybrid pedestrian positioning system using the combination of wearable inertial sensors and ultrasonic ranging (H-PPS). A robust two nodes integration structure is developed to adaptively combine the motion data acquired from the single waist-mounted and foot-mounted node, and enhanced by a novel ellipsoid constraint model. In addition, a deep-learning-based walking speed estimator is proposed by considering all the motion features provided by different nodes, which effectively reduces the cumulative error originating from inertial sensors. Finally, a comprehensive data and model dual-driven model is presented to effectively combine the motion data provided by different sensor nodes and walking speed estimator, and multi-level constraints are extracted to further improve the performance of the overall system. Experimental results indicate that the proposed H-PPS significantly improves the performance of the single PPS and outperforms existing algorithms in accuracy index under complex indoor scenarios.

1. Introduction

Accurate indoor pedestrian positioning system (I-PPS) has a huge application potential towards various merging fields under Global Navigation Satellite System (GNSS) denied urban areas, for example, smart healthcare [1], emergency rescue [2], and motion tracking [3].

At this stage, there are two main approaches for realizing I-PPS: The utilization of additional equipment assisted localization systems and autonomous localization systems is widespread. Among additional equipment assisted localization systems, Wireless Fidelity (Wi-Fi) [4], Bluetooth Low Energy (BLE) [5], ultra-wideband (UWB) [6], acoustic source [7], 5th generation mobile networks (5G) [8], and built-in sensors [9] are the most prominent technologies utilized. These technologies offer public users centimeter-level to room-level localization precision. These types of positioning systems have a few limitations. They require local facilities to generate navigation databases or acquire wireless signals, which are substantially affected by the dynamic and intricate indoor scenes as well as the artificial magnetic field. Specifically, in extremely challenging subterranean or indoor scenarios, with no adequate installed wireless stations and supporting facilities, these systems fail to realize effective and accurate indoor localization performance. Thus, they are required to be combined with additional autonomous positioning sources for better localization performance.

Autonomous positioning systems typically comprise sequence matching using collected magnetic vector [10], simultaneous localization and mapping (SLAM) [11], and multi-source fusion using multiple sensors [12]. In which, sequence matching is realized by comparing magnetic features between collect vector and

* Corresponding author.
E-mail address: michael-yue.yu@polyu.edu.hk (Y. Yu).
Peer review under responsibility of China Ordnance Society

https://doi.org/10.1016/j.dt.2023.11.006

reference vector, that does not need additional facilities. However, at present, magnetic field matching algorithm structures need a period of magnetic data, and changes in building structures and electronic device interference can significantly affect the local magnetic field [13]. For indoor areas with limited features, for instance, long corridors and tunnels, feature extraction and matching difficulties may arise, leading to reduced positioning accuracy. Additionally, visual positioning methods are impacted by light intensity and motion posture, making them unsuitable when applied in case of complex and unpredictable human localization [14]. For distributed inertial positioning systems, IMU equipment in different accuracy indexes is deployed on various locations of the human body, for instance, foot, waist, arms, and thigh, to enable motion and position tracking. Inertial sensors-based dead reckoning (IS-DR) frameworks can achieve precise localization performance without requiring additional facilities, which is expected to maintain localization accuracy under signal-denied areas.

At this stage, IS-DR typically comprises two position update algorithms: pedestrian dead reckoning (PDR) [15] and inertial navigation system (INS) [16]. The PDR framework involves four stages: gait detection, gait-length calculation, heading estimation, and position cumulation. However, the PDR structure's drawback is that the precision of the estimated location is affected by the variability in handheld modes and individuals' motion features. In contrast to the PDR structure, the INS mechanization is not influenced by users' changeable motion and handheld modes, but its error quickly diverges when no effective constraints are applied.

For motion tracking applications, the wearable inertial sensors-based localization system could be divided into the single node based positioning system and multi-nodes based positioning system. Normally, single node based positioning system usually contains the foot-mounted positioning system (FPS) and waist-mounted positioning system (WPS), which are two main existing real-world applications. The challenge of the single node based positioning system is that the node installation of the single location cannot fully describe the motion features of the pedestrian, and its performance is also limited by the cumulative error such as systematic heading deviation and walking speed drift [17]. To enhance the accuracy of the single node-based positioning framework, multi-nodes are applied for positioning error constraints. The most typical application is the dual foot-mounted positioning system (D-FPS), that can significantly reduce the systematic heading deviation and the application of inner foot-ranging can further increase the precision of walking speed calculation. Niu et al. [18] proposed a robust data integration approach based on dual foot-mounted modules in order to decrease the systematic heading error originating from the single FPS. The multi-level equality control algorithm is adopted to integrate the motion features of different system without additional ranging device. Zhu et al. [19] used ultrasonic ranging to get the real-time distance between two feet, and further integrate the inner feet ranging results with dual inertial foot-mounted data under Earth frame to conquer the challenges of systematic heading error and inaccurate performance of walking speed calculation.

In addition, the integration of foot-mounted nodes and the waist-mounted node can provide a more comprehensive motion description of the pedestrian, and the corporation of different nodes can acquire much more motion constraints and improve the heading and walking speed calculation accuracy. Yu et al. [20] compared the localization performance of foot-mounted, waist-mounted, and handheld inertial sensors, and several state-of-art filters are adopted for data fusion respectively. According to the comprehensive experiments, the waist-mounted approach realizes the higher accuracy than other two approaches, and different route path make an important influence for final trajectory. Qiu et al. [21] proposed a wireless inertial motion capture module which uses a number of 15 inertial modules to reconstruct the motion and location of users using unconstrained traversal of the root, and gradient descent algorithm is applied for sensors data fusion, which effectively achieves the error divergence. The problems of existing multi-nodes based positioning systems are that the cumulative heading and walking speed of the users cannot be well constrained due to the low performance of the sensors fusion model. Besides, the indoor artificial magnetic field and complex motion modes would also decrease the precision of heading and pedestrian speed calculation.

To enhance the performance of distributed inertial nodes based positioning system, this paper develops a hybrid pedestrian positioning system using the combination of wearable inertial sensors and ultrasonic ranging (H-PPS), which can maintain positioning precision under the effects of complex user motion modes and artificial interference. The main contributions of this work are summarized as:

(1) This paper applied multi-level observation constrains to eliminate the cumulative error originating from the INS algorithm, which autonomously estimates and compensates for the bias error of inertial sensors and can maintain the precision of the single node-based positioning system.
(2) This paper develops a robust two nodes integration structure to adaptively combine the motion data acquired from the single waist-mounted and foot-mounted nodes, which contains the dual feet and ultrasonic fusion structure and foot-waist fusion structure, and are further enhanced by a novel ellipsoid constraint model.
(3) This paper proposes a deep-learning-based walking speed estimator using the combination of 1D-CNN, Bi-LSTM, and MLP models, which considers all the motion features provided by different inertial nodes and effectively reduces the cumulative error originating from inertial sensors.
(4) This paper presents a comprehensive data and model dual-driven model to adaptively combine the motion data provided by different sensor nodes and walking speed estimator, and multi-level constraints are extracted to further enhance the precision of the overall system.

The structure of this article is arranged as follows. Section 2 presents the single and dual nodes-based positioning systems and models. Section 3 proposes a robust walking speed estimator and final multi-node integration structure. Section 4 designs comprehensive experiments to verify the proposed H-PPS. Section 4 summarizes the whole work and point out the future work.

2. Single and dual nodes positioning system

In this section, the single and dual nodes-based positioning systems are presented progressively for pedestrian navigation. In which the single node positioning system (S-NPS) contains the foot-mounted and waist-mounted positioning systems respectively, and the dual nodes positioning system (D-NPS) is the combination of different S-NPS. The overall structure of proposed H-PPS system is described in Fig. 1.

2.1. Single node based positioning model

In the S-NPS, the foot-mounted and waist-mounted positioning

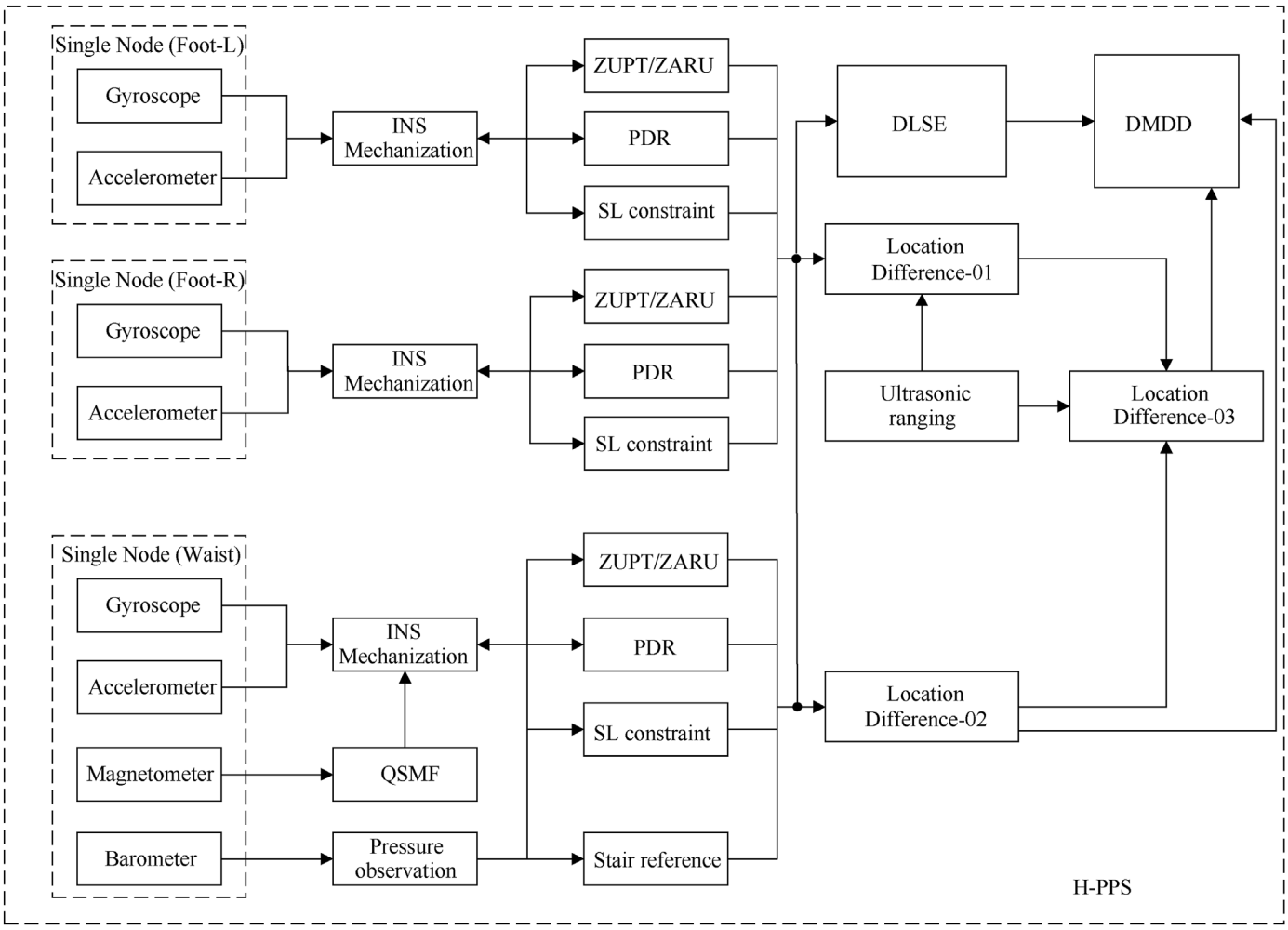

Fig. 1. Overall Structure of proposed H-PPS.

systems have the common part of INS mechanization aimed attitude and position updating algorithm, and also have the specific observations of each. The common part of INS mechanization-based attitude and location update method is summarized as [17]

$$(\dot{\boldsymbol{p}}^n, \dot{\boldsymbol{v}}^n, \dot{\boldsymbol{C}}_b^n) = \begin{cases} \varpi^{-1}\boldsymbol{v}^n \\ \boldsymbol{C}_b^n \boldsymbol{f}^b - (2\boldsymbol{\omega}_{ie}^n + \boldsymbol{\omega}_{en}^n)\boldsymbol{v}^n + \boldsymbol{g}^n \\ \boldsymbol{C}_b^n \left(\boldsymbol{\omega}_{ib}^b + \boldsymbol{\omega}_{in}^b\right) \end{cases} \tag{1}$$

where $\boldsymbol{p}^n = [\,p_N \quad p_E \quad p_D\,]^{\mathrm{T}}$ and $\boldsymbol{v}^n = [\,v_N \quad v_E \quad v_D\,]^{\mathrm{T}}$ indicate the cumulated 3D position and speed information of S-NPS in n-frame; $\boldsymbol{C}_b^n$ indicates the current rotation matrix; $\boldsymbol{g}^n$ is the acquired gravity vector; $\boldsymbol{\omega}_{ie}^n$ and $\boldsymbol{\omega}_{en}^n$ indicate the measured rotation angular rates among Earth-centered Earth-fixed frame and i-frame, between n-frame and the ECEF frame.

The Earth rotation related parameters $\boldsymbol{\omega}_{ib}^b$ and $\boldsymbol{\omega}_{in}^b$ can be simplified because of the low accuracy level of MEMS sensors integrated in S-NPS, as shown below [18]:

$$\begin{cases} \delta\dot{\boldsymbol{p}}^n = -\boldsymbol{\omega}_{en}^n \times \delta\boldsymbol{p}^n + \delta \\ \delta\dot{\boldsymbol{v}}^n = -(2\boldsymbol{\omega}_{ie}^n + \boldsymbol{\omega}_{en}^n)\delta\boldsymbol{v}^n + \boldsymbol{f}^n \times \boldsymbol{\psi} + \boldsymbol{C}_b^n(\boldsymbol{\varepsilon}_a + \boldsymbol{w}_{ba}) \\ \dot{\boldsymbol{\psi}} = -(\boldsymbol{\omega}_{ie}^n + \boldsymbol{\omega}_{en}^n) \times \boldsymbol{\psi} - \boldsymbol{C}_b^n\left(\boldsymbol{\varepsilon}_g + \boldsymbol{w}_{bg}\right) \\ \dot{\boldsymbol{\varepsilon}}_g = \boldsymbol{\varepsilon}_g \big/ \tau_{bg} + \boldsymbol{w}_{bg} \\ \dot{\boldsymbol{\varepsilon}}_a = -\boldsymbol{\varepsilon}_a/\tau_{ba} + \boldsymbol{w}_{ba} \end{cases} \tag{2}$$

where $\delta\boldsymbol{p}^n$, $\delta\boldsymbol{v}^n$ and $\boldsymbol{\psi}$ represent the state error of S-NPS contains 3D position, velocity, and attitude vectors; $\boldsymbol{\varepsilon}_g$ and $\boldsymbol{\varepsilon}_a$ is the sensors biases; $\boldsymbol{f}^n$ is the collected acceleration information in n-frame; $\boldsymbol{w}_{bg}$ and $\boldsymbol{w}_{ba}$ are the noises of gyroscope and accelerometer.

Thus, the state vector of S-NPS is described as follows:

$$\delta\boldsymbol{X} = \left[\,(\delta\boldsymbol{p}^n)_{1\times3} \quad (\delta\boldsymbol{v}^n)_{1\times3} \quad \boldsymbol{\psi}_{1\times3} \quad (\boldsymbol{\varepsilon}_g)_{1\times3} \quad (\boldsymbol{\varepsilon}_a)_{1\times3}\,\right]^{\mathrm{T}} \tag{3}$$

The proposed S-NPS also contains ZUPT and ZARU observations when the quasi-static (QS) period is detected, in which the ZUPT observation is defined as:

$$\delta \boldsymbol{Z}_v^n = \boldsymbol{v}_{\mathrm{INS}}^n - \boldsymbol{v}_{\mathrm{zero}}^n = \delta v^n + n_v \tag{4}$$

where $\boldsymbol{v}_{\mathrm{INS}}^n$ jun is S-NPS originated speed vector, $\boldsymbol{v}_{\mathrm{zero}}^n = [0 \quad 0 \quad 0]^{\mathrm{T}}$ is ideal observation vector. While the ZUPT cannot eliminate the heading drift under QS period, thus the ZARU algorithm is also applied for heading calibration [4]

$$\delta \boldsymbol{Z}_\theta = \theta_{\mathrm{INS}}^n + \theta_{\mathrm{refer}}^n = \delta\theta + n_\theta \tag{5}$$

where θ_{INS}^n is the S-NPS provided heading value, $\theta_{\mathrm{refer}}^n$ is extracted reference heading observation among QS period, and n_θ represents the measurement noise.

To decrease the divergence error under non-QS periods, the PDR originated gait-length and velocity measurements are also adopted as the observation equation in our developed S-NPS [17]:

$$\boldsymbol{V}_{\mathrm{PDR}} = [\alpha_s/(\mu_1 - \mu_0) \quad 0 \quad 0] \tag{6}$$

where $\boldsymbol{V}_{\mathrm{PDR}}$ indicates the PDR calculated gait-length value. μ_1 and μ_0 are the collected time indexes of detected gait, and the PDR is also applied for location update for the error constraint of proposed S-NPS:

$$\begin{bmatrix} r_x^t \\ r_y^t \end{bmatrix} = \begin{bmatrix} r_x^{t-1} \\ r_y^{t-1} \end{bmatrix} + \int_{t-1}^{t} \boldsymbol{V}_{\mathrm{PDR}}(k) \begin{bmatrix} \cos\theta_k \\ \sin\theta_k \end{bmatrix} \mathrm{d}k \tag{7}$$

where r_x^t and r_y^t indicate the 2D position, θ_k is the S-NPS originated heading observation.

Therefore, the PDR-assisted constraint model is described as

$$\begin{cases} \delta \boldsymbol{Z}_{\boldsymbol{v}} = \boldsymbol{v}_{\mathrm{pdr}} - \boldsymbol{v}_{\mathrm{s-NPS}} \\ \delta \boldsymbol{Z}_{\boldsymbol{P}} = \boldsymbol{P}_{\mathrm{pdr}} - \boldsymbol{P}_{\mathrm{s-NPS}} \end{cases} \tag{8}$$

where $\boldsymbol{v}_{\mathrm{pdr}}$ and $\boldsymbol{P}_{\mathrm{pdr}}$ indicates the PDR originated position and speed vectors; $\boldsymbol{v}_{\mathrm{s-NPS}}$ and $\boldsymbol{P}_{\mathrm{s-NPS}}$ are the S-NPS provided speed and position vector.

To enhance the positioning performance, the straight-line (SL) constraint is extracted to limit the divergence error under the regular walking route. This technique has been demonstrated to significantly enhance the localization accuracy of S-NPS [22]. Moreover, in this research, heading information calculated from adjacent gait periods is recorded for straight-line recognition.

$$L_1 = \begin{cases} 1 & \max\{|\boldsymbol{\theta}^s - \mathrm{mean}(\boldsymbol{\theta}^s)|\} < \boldsymbol{T}_{1,\theta} \\ 0 & \text{others} \end{cases} \tag{9}$$

$$\begin{cases} \boldsymbol{\theta}^s = \{\boldsymbol{\theta}_{m-4}^s, \boldsymbol{\theta}_{m-3}^s, \cdots, \boldsymbol{\theta}_m^s\} \\ \boldsymbol{\theta}_m^s = a\tan 2\left(\boldsymbol{r}_{y,m}^n - \boldsymbol{r}_{y-1,m}^n, \boldsymbol{r}_{x,m}^n - \boldsymbol{r}_{x,m-1}^n\right) \end{cases} \tag{10}$$

where $(\boldsymbol{r}_{x,m}^n, \boldsymbol{r}_{y,m}^n)$ represents the mth step position calculated by S-NPS, if $L_1 = 1$, the user is recognized as walking alongside a straight network. Therefore, the observation equation is defined as

$$\frac{\boldsymbol{\theta}_m^s - \boldsymbol{\theta}_{m-4}^s}{\Delta t} = [\boldsymbol{0}_{1\times 13} \quad \sec\theta\sin\varphi \quad \sec\theta\cos\varphi]\boldsymbol{x}_t + \varepsilon_\psi \tag{11}$$

where θ and φ represent the roll and pitch angles provided by S-NPS, ε_ψ is the heading deviation.

For the waist-mounted positioning system, more sensors are integrated for instance magnetometer and barometer, due to the more stable characteristics of collected motion data compared with the foot-mounted positioning system. Thus, the magnetic feature constraint, stair reference, and pressure-originated altitude observation are applied in the waist-mounted positioning system, in which the magnetic feature constraint is described the following Eq. (34) in final H-PPS.

In a three-dimensional (3D) scenarios with a varies of floors, altitude estimation becomes particularly essential, particularly when pedestrians ascend or descend stairs. In this study, stair-extracted altitude observation is selected and modeled to limit the divergence of the S-NPS provided altitude.

$$\delta \boldsymbol{Z}_h = h_{\mathrm{stair}} - h_{\mathrm{S-NPS}} \tag{12}$$

where h_{stair} represents the updated altitude using reference height of stairs, $h_{\mathrm{S-NPS}}$ represents the S-NPS provided altitude.

While the performance of attitude calculation using S-NPS will cumulate quickly, therefore, for the waist-mounted positioning system, the barometer provided altitude constraint is also extracted for divergence error control [12].

$$\delta \boldsymbol{z}_h^n = h_B^n - h_{\mathrm{INS}}^n \tag{13}$$

where h_B^n indicates the barometer-originated altitude calculation value presented in Eq. (13), h_{INS}^n indicates the z-axis location change estimated by S-NPS.

2.2. Dual nodes based positioning model

As defined in the above section, the S-NPS commonly comprises an INS algorithm, QS recognition model, and multi-level constraints for ZUPT/ZARU and straight-line constraint. However, due to the difficulty of eliminating the systematic heading drift originating from the S-NPS, a dual nodes positioning system (D-NPS) is developed to constrain the systematic heading drift to the greatest extent possible when using S-NPS. The proposed D-NPS contains three different integration models of S-NPS: the dual foot-mounted modules without ultrasonic ranging (DFM-NU), the dual foot-mounted modules with ultrasonic ranging (DFM-U), the hybrid foot-mounted and waist-mounted modules (H-FWM). For the overall algorithm model of D-NPS, the basic state vector is modeled using the two subsystems of both the left and right foot nodes or a combination of foot and waist nodes

$$\boldsymbol{X}^{\mathrm{All}} = [\boldsymbol{X}^{(01)} \quad \boldsymbol{X}^{(02)}] \tag{14}$$

where $\boldsymbol{X}^{(01)}$ and $\boldsymbol{X}^{(02)}$ represent the foot-mounted or the waist-mounted S-NPS. Therefore, the final state vector of D-NPS is the combination of two different S-NPS

$$\delta \boldsymbol{X}_i^{\mathrm{All}} = \boldsymbol{F}_{i-1}\delta \boldsymbol{X}_i^{\mathrm{All}} + \boldsymbol{G}_{i-1}\boldsymbol{w}_{i-1}^{\mathrm{All}} \tag{15}$$

where $\boldsymbol{w}_{i-1}^{\mathrm{All}}$ is measurement noises under the Gaussian distribution; $\boldsymbol{F}_{i-1}$ represents the augmented state matrix, and $\boldsymbol{G}_{i-1}$ is the augmented noise gain matrix, which are described as follows

$$\boldsymbol{F} = \begin{bmatrix} \boldsymbol{F}^{(01)} & \boldsymbol{0}_{15,15} \\ \boldsymbol{0}_{15,15} & \boldsymbol{F}^{(02)} \end{bmatrix}, \boldsymbol{G} = \begin{bmatrix} \boldsymbol{G}^{(01)} & \boldsymbol{0}_{15,15} \\ \boldsymbol{0}_{15,15} & \boldsymbol{G}^{(02)} \end{bmatrix} \tag{16}$$

For the dual foot-mounted positioning system (D-FPS), among the detected QS period of one foot, the other foot is just detected as the moving status, which is shown as.

Fig. 2 indicates that the left and the right foot prove the temporal complementarity of detected QS periods.

For the D-NPS, the relationship between foot-mounted nodes and waist-mounted node is described in Fig. 2. Where the ellipse

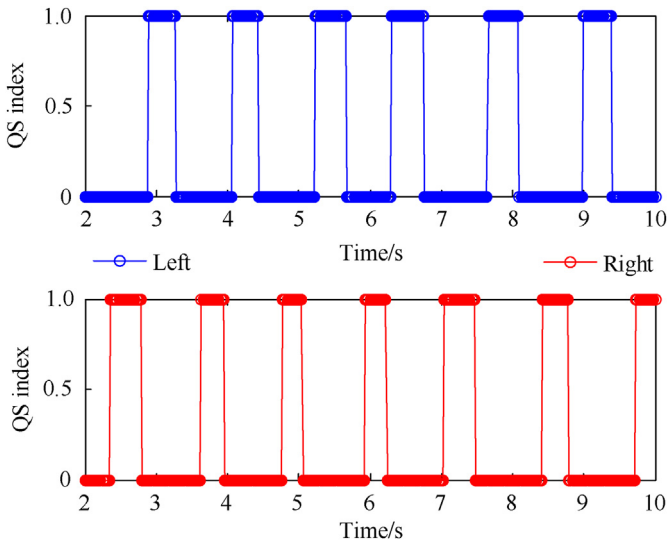

Fig. 2. Recognized QS Periods using D-FPS.

constraint is applied in ideal case, the central of the ellipse is modeled as the 2D position of the waist-mounted module, and the semi-major axis of the ellipse is the distance between 2D location of the waist-mounted module and two foot-mounted modules. In the ideal case, the distances between 2D location of the waist-mounted module and two foot-mounted modules R_1, R_2 are the same, and the distance between two foot-mounted modules is also measured by the ultrasonic ranging D_{ultra}.

In Fig. 3, the ultrasonic ranging measurements can be adopted as the multi-level observed constraints combined with the locations of waist-mounted and foot-mounted modules in order to decrease the speed divergence and positioning deviation. Firstly, for the dual foot-mounted combination, the observation model can be constructed as [17].

$$\delta \boldsymbol{Z}_{01} = \|D_{\text{FPS}} - D_{\text{ultra}}\| \tag{17}$$

in the equation, $\boldsymbol{Z}$ represents the deviation among the ranging result distance between the left and right foot by the ultrasonic signal and S-NPS. Based on step analysis of the D-FPS, the distance among two feet is not constant and is defined as

$$D_{\text{FPS}} = \|\boldsymbol{H}\boldsymbol{X}_i\| + \omega_i \tag{18}$$

where

$$\boldsymbol{H} = \begin{bmatrix} \boldsymbol{I}_3 & \boldsymbol{0}_{3,12} & -\boldsymbol{I}_3 & \boldsymbol{0}_{3,12} \end{bmatrix} \tag{19}$$

in the final integration phase, an ultrasonic outlier detector is used to identify and remove detected outliers from the observations. This process helps remain the localization precision of the final D-FPS.

Secondly, for the hybrid waist-mounted and foot-mounted positioning system, the observation model can be constructed as:

$$\delta \boldsymbol{Z}_{02} = \|R_1 - R_2\| \tag{20}$$

where

$$R_{1/2} = \sqrt{\left(x_0 - x_{1/2}\right)^2 + \left(y_0 - y_{1/2}\right)^2} \tag{21}$$

In Eq. (22), (x_0, y_0) indicates the 2D location of waist-mounted module, (x_1, y_1) and (x_2, y_2) represent the locations of two foot-mounted modules.

Thirdly, the distance between waist-mounted module and two foot-mounted modules also has the following constraints:

$$\delta \boldsymbol{Z}_{03} = \|R_1 + R_2 - D_{\text{ultra}}\| \tag{22}$$

The difference of calculated distances provided by ultrasonic ranging and waist-mounted and foot-mounted nodes will be equal under the ideal walking mode.

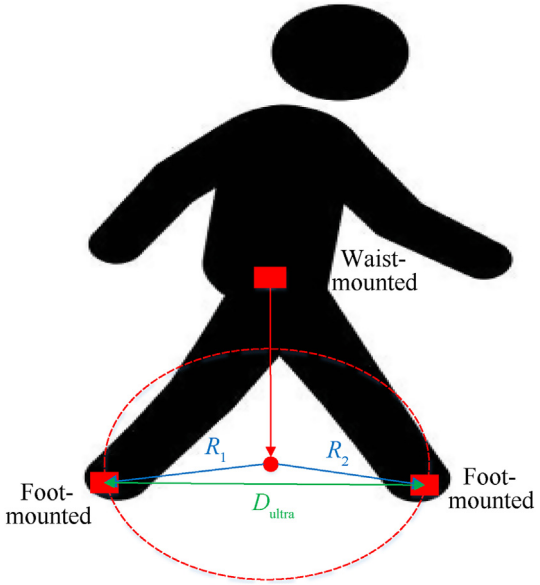

Fig. 3. Model of dual nodes based positioning.

3. Hybrid nodes based positioning system

In this section, the subsystems of waist-mounted and foot-mounted modules are integrated together for a robust estimation of human motions and locations. A novel walking speed estimator is designed to provide accurate pedestrian speed information using hybrid nodes. In addition, a data and model dual-driven model is developed for collaborative localization using different modules.

3.1. Hybrid walking speed estimator

The performance of single node based positioning system is limited by the complex human motion and cumulative error. In this section, a robust deep-learning-based speed estimator (DLSE) combining features extracted from different nodes is developed to provide precise walking speed reference regarding the above challenges. In this work, a hybrid deep-learning based walking speed estimation structure is developed by considering motion features extracted from a period of sensor data and ultrasonic ranging results from different inertial nodes instead of instantaneous model in formal researches. The network structure of the developed DLSE framework contains the integration of one-dimensional convolutional neural network model (1D-CNN), Bi-directional Long Short-Term Memory (Bi-LSTM), and multilayer perceptron (MLP) which is shown as follows:

Fig. 4 describes the basic model of proposed DLSE framework, in which the 1D-CNN is adapted to fully learn and extract the motion features of the users, and the Bi-LSTM network further takes the time-related characteristics into consideration, and MLP is finally applied to integrate all the learned features and predict overall

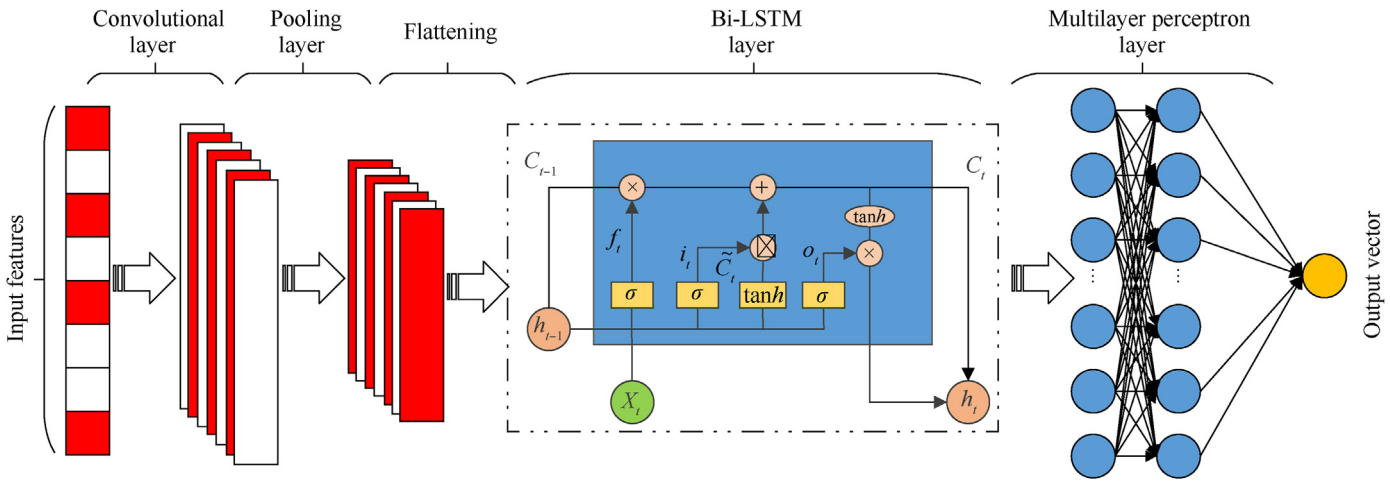

Fig. 4. Hybrid deep-learning framework.

walking speed for users.

In the 1D-CNN module, the relationship among the input features and the outputted learned features is defined as [23]:

$$O_j = \varpi\left(\sum_{i=1}^{N} x_i k_{ij} + b_j\right) \tag{23}$$

where x_i is the modeled input features, k_{ij} is the kernel weights, b_j is the calculated biases, $\varpi(\cdot)$ is the activation function, and O_j is the learned output features of 1D-CNN.

Among the Bi-LSTM module, the updated parameters of Bi-LSTM network are defined as [17]:

$$\begin{cases} f_t = \sigma\left(W_f[h_{t-1}, X_t] + b_f\right) \\ i_t = \sigma(W_i \cdot [h_{t-1}, X_t] + b_i) \\ \tilde{C}_t = \tanh(W_C \cdot [h_{t-1}, X_t] + b_C) \\ o_t = \sigma(W_o[h_{t-1}, X_t] + b_o) \\ h_t = o_t \tanh(C_t) \end{cases} \tag{24}$$

where i_t, f_t, o_t indicate the input, forget and output units, X_t indicates the input vector of Bi-LSTM model at the timestamp t, and the h_t represents the hidden state vector, which is regarded as the output of the Bi-LSTM model at that moment. σ indicates the sigmoid function, and C_t is the candidate vector which is combined with output vector as the memorized state at timestamp t.

Then the output vector of the proposed Bi-LSTM network is adopted as the input vector of MLP module, and the final predicted walking speed information is defined as:

$$v_t = MLP(h_t) \tag{25}$$

In which v_t indicates the final predicted walking speed provided by the proposed DLSE.

To get better performance of speed estimation, following features are extracted to adaptively describe the motion characteristics of the pedestrian wearing hybrid inertial nodes:

(1) Foot-mounted modules estimated walking speed values v_1 and v_2, respectively;
(2) Ranging distance results u_1 provided by ultrasonic module;
(3) Ranging difference u_2 calculated by ultrasonic module;
(4) Walking speed vector calculated by the waist-mounted node by the linear model:

$$L_1 = \frac{\alpha[0.7 + \beta(H - 1.75) + \varsigma(F_t - 1.79)H/1.75]}{t_1 - t_0} \tag{26}$$

In which the α, β, ς indicate the human feature-related parameters, F_t represents the step frequency, and H indicates the user's height value.

(5) Walking speed vector calculated by the waist-mounted node by the non-linear model:

$$L = K\sqrt[4]{A_{\max} - A_{\min}} \tag{27}$$

where $A_{\max}$ and $A_{\min}$ represent the recognized peak and valley vectors acquired from acceleration under the detected step period, K indicates the scale parameters for different users.

(6) Norm of collected accelerometer data provided by the waist-mounted module:

$$Norm_{\text{acc}} = \sqrt{a_x^2 + a_y^2 + a_z^2} \tag{28}$$

(7) Norm of collected angular rate data provided by the waist-mounted module

$$Norm_{\text{gyro}} = \sqrt{g_x^2 + g_y^2 + g_z^2} \tag{29}$$

(8) Update frequency F_t of step-length calculated by the waist-mounted node.

The output dimension of proposed DLSE only contains 1D walking speed prediction result described in Eq. (25), which is further applied as one of the observations in the further data and model dual-driven based fusion model.

3.2. Data and model dual-driven positioning model

In this part, a unified data and model dual-driven (DMDD) model is developed based on the consideration of motion information provided by hybrid inertial nodes, magnetic reference, and DLSE result, which achieves a comprehensive integration for MEMS sensors-based user localization. The state vector of each subsystem

is modeled as [19]

$$\delta \boldsymbol{X}_{\text{sub}}^{i} = \left[\begin{array}{cccc} (\delta \boldsymbol{p}^{n})_{1\times 3} & (\delta \boldsymbol{v}^{n})_{1\times 3} & \boldsymbol{\varphi}_{1\times 3} & \left(\boldsymbol{\varepsilon}_{g}^{b}\right)_{1\times 3} \quad \left(\nabla_{a}^{b}\right)_{1\times 3} \end{array} \right]^{\mathrm{T}} \tag{30}$$

where $\delta \boldsymbol{p}^{n}$, $\delta \boldsymbol{v}^{n}$ and $\boldsymbol{\varphi}$ indicate the state error of position, velocity, and attitude under n-frame. $\boldsymbol{\varepsilon}_{g}$ and ∇_{a} are the biases of the gyroscope and accelerometer. For the final H-PPS, the basic system state vector is modeled using the information acquired from three subsystems including feet nodes and waist node

$$\boldsymbol{X}^{\text{Hybrid}} = \left[\begin{array}{ccc} \boldsymbol{X}_{F}^{(01)} & \boldsymbol{X}_{F}^{(02)} & \boldsymbol{X}_{W} \end{array} \right] \tag{31}$$

where $\boldsymbol{X}_{F}^{(01)}$ and $\boldsymbol{X}_{F}^{(02)}$ indicate the foot-mounted subsystems, $\boldsymbol{X}_{W}$ is the waist-mounted subsystem. Each component comprises a rank of 15 state vector defined in Eq. (31), and the state vector of whole H-PPS is defined as

$$\delta \boldsymbol{X}_{i}^{\text{Hybrid}} = \boldsymbol{F}_{i} \delta \boldsymbol{X}_{i-1}^{\text{Hybrid}} + \boldsymbol{G}_{i} \boldsymbol{w}_{i-1}^{\text{Hybrid}} \tag{32}$$

where $\boldsymbol{F}_{i}$ is the state transition matrix, $\boldsymbol{G}_{i}$ represents the noise gain matrix.

The original INS mechanization is subjected to the cumulative and divergence errors originated from low-cost sensors, thus cannot be applied individually. In the proposed DMDD structure, the DLSE predicted walking speed and updated information is applied as the observations.

$$\begin{cases} \delta \boldsymbol{Z}_{v}^{n} = \boldsymbol{v}_{\text{DLSE}}^{n} - \boldsymbol{v}_{\text{INS}}^{n} \\ \delta \boldsymbol{Z}_{p}^{n} = \boldsymbol{p}_{\text{DLSE}}^{n} - \boldsymbol{p}_{\text{INS}}^{n} \end{cases} \tag{33}$$

where $\boldsymbol{v}_{\text{DLSE}}^{n}$ and $\boldsymbol{p}_{\text{DLSE}}^{n}$ represent DLSE predicted walking velocity and position measurements, $\boldsymbol{v}_{\text{INS}}^{n}$ and $\boldsymbol{p}_{\text{INS}}^{n}$ represent the walking speed and location calculated by INS mechanization. The DLSE based position reference $\boldsymbol{p}_{\text{DLSE}}^{n}$ is calculated based on the walking speed prediction result $\boldsymbol{v}_{\text{DLSE}}^{n}$ and the last moment position information provided by the final DMDD structure. To decrease the effect of the distorted local magnetic field, in this work, the magnetic measurement of waist-mounted module among the recognized quasi-static magnetic field (QSMF) is extracted for modeling the difference vector between the first epoch data [5]:

$$\delta \boldsymbol{Z}_{m}^{n} = C_{n,k}^{b} \boldsymbol{m}_{k}^{b} - C_{n,1}^{b} \boldsymbol{m}_{k,1}^{b} \tag{34}$$

where $C_{n,1}^{b}$ and $\boldsymbol{m}_{k,1}^{b}$ indicate the attitude matrix and magnetic data collected from the first QSMF epoch, $C_{n,k}^{b}$ and $\boldsymbol{m}_{k}^{b}$ indicate the attitude matrix and magnetic data collected from the following QSMF epochs.

In this work, UKF is applied for data fusion of modeled H-PPS structure, and the main steps of UKF are defined as:

(1) Initialization process for state vector:

$$\begin{cases} \widehat{\boldsymbol{X}}_{0} = E[\boldsymbol{X}_{0}] \\ \boldsymbol{P}_{0} = E\left[[\boldsymbol{X}_{0} - \widehat{\boldsymbol{X}}_{0}][\boldsymbol{X}_{0} - \widehat{\boldsymbol{X}}_{0}]^{\mathrm{T}} \right] \end{cases} \tag{35}$$

(2) Update the sigma point set:

$$\boldsymbol{X}_{k-1} = \left[\widehat{\boldsymbol{X}}_{k-1}, \widehat{\boldsymbol{X}}_{k-1} + \gamma \sqrt{\boldsymbol{P}_{k-1}}, \widehat{\boldsymbol{X}}_{k-1} - \gamma \sqrt{\boldsymbol{P}_{k-1}} \right] \tag{36}$$

where $\boldsymbol{P}_{k\text{-}1}$ is the covariance matrix calculated at last moment, γ is the set proportional parameter.

(3) State vector prediction and observation integration:

$$\boldsymbol{X}_{k|k-1}^{i} = \boldsymbol{\varphi} \boldsymbol{X}_{k-1}^{i} \tag{37}$$

$$\boldsymbol{X}_{k}^{-} = \sum_{i=0}^{2n+1} \omega_{i} \boldsymbol{X}_{k|k-1}^{i} \tag{38}$$

$$\boldsymbol{P}_{k}^{-} = \sum_{i=0}^{2n+1} \omega_{i} \left(\boldsymbol{X}_{k|k-1}^{i} - \widehat{\boldsymbol{X}}_{k}^{-} \right) \left(\boldsymbol{X}_{k|k-1}^{i} - \widehat{\boldsymbol{X}}_{k}^{-} \right) + \boldsymbol{G} \boldsymbol{Q}_{k} \boldsymbol{G}^{\mathrm{T}} \tag{39}$$

$$\boldsymbol{Z}_{k|k-1}^{i} = h\left(\boldsymbol{X}_{k|k-1}^{i} \right) \tag{40}$$

$$\boldsymbol{z}_{k}^{-} = \sum_{i=0}^{2n+1} \omega_{i} \boldsymbol{Z}_{k|k-1}^{i} \tag{41}$$

(4) Observation parameter update:

$$\boldsymbol{P}_{\tilde{z}k,\tilde{z}k} = \sum_{i=0}^{2n+1} \omega_{i} \left(\boldsymbol{Z}_{k|k-1}^{i} - \widehat{\boldsymbol{z}}_{k}^{-} \right) \left(\boldsymbol{Z}_{k|k-1}^{i} - \widehat{\boldsymbol{z}}_{k}^{-} \right) + \boldsymbol{R}_{k} \tag{42}$$

$$\boldsymbol{P}_{xk,zk} = \sum_{i=0}^{2n+1} \omega_{i} \left(\boldsymbol{X}_{k|k-1}^{i} - \widehat{\boldsymbol{x}}_{k}^{-} \right) \left(\boldsymbol{Z}_{k|k-1}^{i} - \widehat{\boldsymbol{z}}_{k}^{-} \right)^{\mathrm{T}} \tag{43}$$

$$\boldsymbol{K}_{k} = \boldsymbol{P}_{xk,zk} \boldsymbol{P}_{\tilde{z}k,\tilde{z}k}^{-1} \tag{44}$$

$$\widehat{\boldsymbol{x}}_{k} = \widehat{\boldsymbol{x}}_{k}^{-} + \boldsymbol{K}_{k} \left(\boldsymbol{z}_{k} - \widehat{\boldsymbol{z}}_{k}^{-} \right) \tag{45}$$

$$\boldsymbol{P}_{k} = \boldsymbol{P}_{k}^{-} - \boldsymbol{K}_{k} \boldsymbol{P}_{\tilde{z}k,\tilde{z}k} \boldsymbol{K}_{k}^{\mathrm{T}} \tag{46}$$

(5) For the trajectory estimated between two known landmarks or in case of loop point detected [22], the Rauch–Tung–Striebel smoother (RTS) based trajectory optimization algorithm is applied to acquire the high-accuracy smoothed trajectory information:

$$\widehat{\boldsymbol{x}}_{k-1|k} = \widehat{\boldsymbol{x}}_{k-1} + \boldsymbol{P}_{k-1} \boldsymbol{\varphi}_{k}^{\mathrm{T}} \left(\boldsymbol{P}_{k-1}^{-} \right)^{-1} \left(\widehat{\boldsymbol{x}}_{k} - \widehat{\boldsymbol{x}}_{k}^{-} \right) \tag{47}$$

$$\boldsymbol{P}_{k-1|k} = \boldsymbol{P}_{k-1} - \left(\boldsymbol{P}_{k-1} \boldsymbol{\varphi}_{k}^{\mathrm{T}} \left(\boldsymbol{P}_{k}^{-} \right)^{-1} \right) \left(\boldsymbol{P}_{k} - \boldsymbol{P}_{k}^{-} \right) \left(\boldsymbol{P}_{k-1} \boldsymbol{\varphi}_{k}^{\mathrm{T}} \left(\boldsymbol{P}_{k}^{-} \right)^{-1} \right)^{\mathrm{T}} \tag{48}$$

in summary, in the final DMDD enhanced H-PPS, to integrate all the motion features provided by different nodes and consider the constraining relationship between different IMU nodes. First of all, the INS mechanization is applied as the basic position-attitude update method, the error values of INS mechanization from all three IMU nodes are modeled together as state vector of H-IPS. Secondly, to further eliminate the cumulative error of INS mechanization, the observations and constraints extracted from multi-sensors and human motion information are applied to decrease

cumulative error at the single node level, including ZUPT/ZARU, PDR, SL, stair and pressure reference. Then the ultrasonic ranging and error ellipse-based location differences constraints are extracted for dual IMU nodes, including foot-mounted and waist-mounted systems. Finally, for the overall H-PPS, DLSE is proposed to predict the walking speed as the observation and DMDD structure is applied to integrate all the state vector, observations and constraints for the optimization of each IMU node and get the optimal positioning results of overall system.

4. Experimental results of FPS-DU

In this section, comprehensive experiments are conducted to verify the precision of the proposed single-node positioning system (S-NPS), dual nodes positioning system (D-NPS), and final H-PPS. Three different indoor and outdoor scenes are chosen as the experimental scenes, and comparison experiments are designed with existing algorithms and systems. Three wearable inertial nodes are deployed at the two feet and the waist of the testers, described in Fig. 5. The accuracy parameters of inertial sensors integrated in the IMU module are described in Table 1.

4.1. Precision estimation of single node-based positioning model

In this work, multi-level observations are extracted to constrain the divergence error of INS mechanization applied in S-NPS. To evaluate the performance, a cross-floor scene is chosen as the experimental scene. Testers started from point A, went through the point B, C, upstairs to the point D, passed the point E-D, downstairs, and return to the point A. The walking duration and walking distance are 335 m and 220 s, respectively. The overall walking route is described in Fig. 6. In this work, all the ground-truth trajectories are acquired by high-precision SLAM system, which can provide centimeter level reference trajectories that can be applied as ground-truth [11].

Table 1
Accuracy parameters of IMU module.

Parameters	Gyroscope	Accelerometer
Sampling rate	100 Hz	100 Hz
Dynamic range	2000°/s	16 g
Bias instability	10°/h	0.03 mg
White noise	$0.16^\circ/\sqrt{h}$	$0.02m/s/\sqrt{h}$

Fig. 7 indicates that the performance of single waist-mounted module is better that the foot-mounted positioning system, and the proposed multi-level observations applied on the S-NPS further enhance the positioning precision by decreasing the cumulative error and drift. The errors comparison between different positioning models are described as Fig. 8.

Fig. 8 describes that the multi-level constraints effectively enhance the performance of raw trajectory provided by S-NPS, and the waist-mounted positioning system realizes the higher accuracy compared with the foot-mounted positioning system. The evaluated positioning error of waist-mounted positioning system reaches 2.1 m in 75% under tested walking route, compared with the foot-mounted positioning system within 3.78 m in 75%. Normally, the foot-mounted IMU can use ZUPT/ZARU to improve the performance of speed estimation and heading divergence, while the ZUPT/ZARU algorithm makes very small contributions for improving the heading accuracy due to the lack of absolute observations. Compared with the foot-mounted IMU, the waist-mounted IMU has more stable acquired sensors data and effective reference of local magnetic observations under complex environments and human motion modes, and the PDR step-length based observations are also more accurate than foot-mounted algorithm. Thus, the accuracy of heading estimation and fused positioning using waist-mounted IMU is higher than foot-mounted IMU.

In addition, we conduct the comparison with other state-of-art algorithms including foot-mounted indoor localization system (FIL) proposed in Ref. [22], and walking step-length assumption method

Fig. 5. Hardware modules of H-PPS.

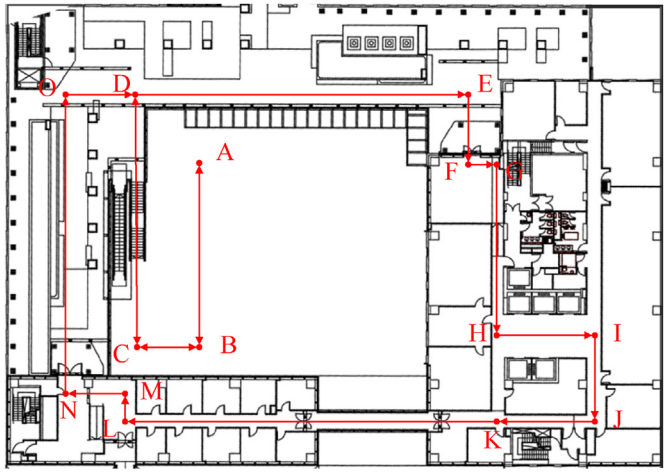

Fig. 6. Walking route of S-NPS evaluation.

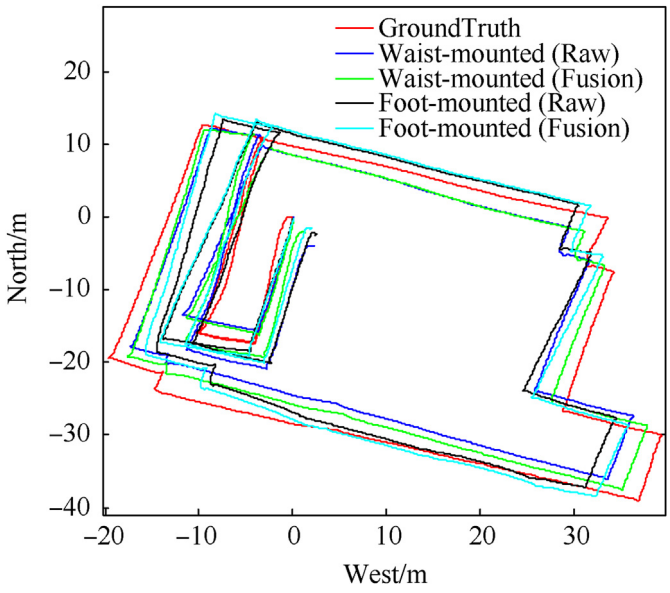

Fig. 7. Walking route of S-NPS evaluation.

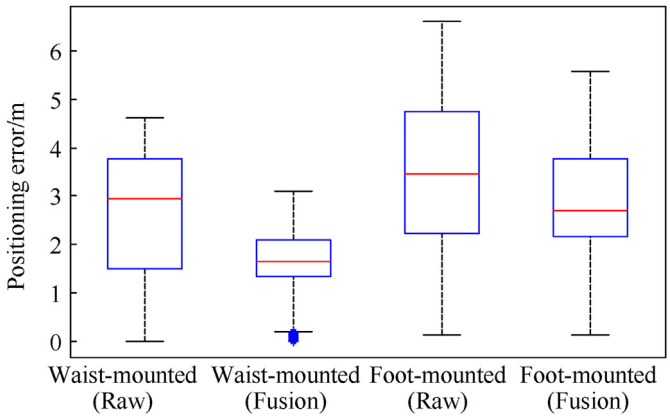

Fig. 8. Errors comparison of different Structure.

(WSA) proposed in Ref. [24]. The performance of waist-mounted positioning system and foot-mounted positioning system are compared respectively under the same walking route. The comparison results is described as Fig. 9.

Fig. 9 presents that the proposed S-NPS structure realizes better positioning performance compared with existing algorithms. The estimated MSA and waist-mounted positioning structure reaches 3.08 m and 2.1 m in 75%, and the FIL and foot-mounted positioning structure reaches 4.94 m and 3.78 m.

4.2. Performance evaluation of dual nodes-based positioning model

Furthermore, we designed experiments to verify the precision of D-NPS, a corridor contained indoor environment is selected as the experimental site. The walking route of testers is described in Fig. 10. The tester started from the point H, passed the point I, J, K, L, F, G and returned to the point H. The walking duration and walking distance are 150 m and 102 s, respectively.

To evaluate the performance of D-NPS using different integration model of single node, the dual foot-mounted modules without ultrasonic ranging (DFM-NU), the dual foot-mounted modules with ultrasonic ranging (DFM-U), the hybrid foot-mounted and waist-

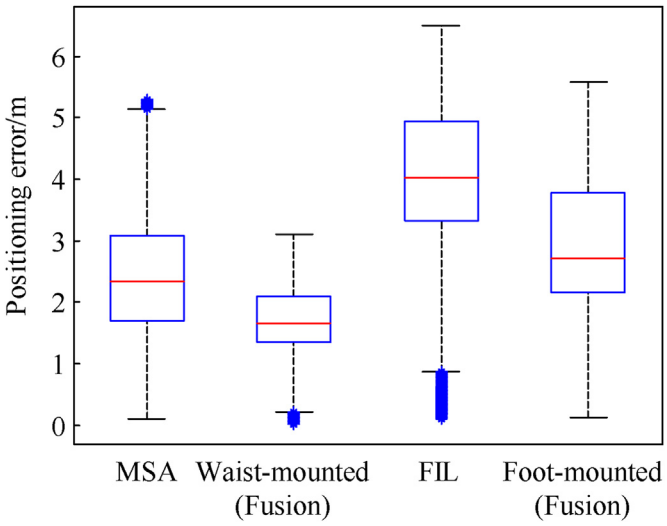

Fig. 9. Errors comparison with existing algorithms.

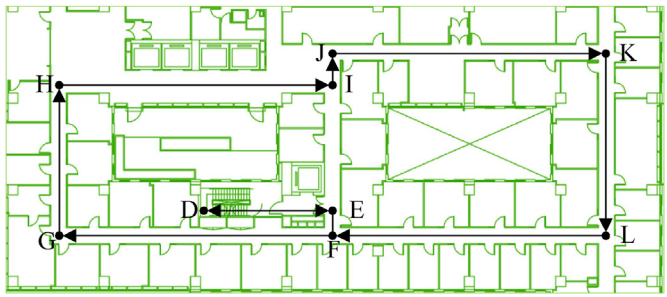

Fig. 10. Walking route in 9th floor.

mounted modules (H-FWM) are evaluated respectively. Firstly, the S-NPS is compared with the DFM-NU and H-FWM, the estimated trajectories and related positioning errors provided by different integration models are described in Fig. 11.

In addition, the DFM-NU is further compared with DFM-U to evaluate the improvement after using ultrasonic ranging. The estimated trajectories and related positioning errors provided by DFM-NU and DFM-U are compared in Fig. 12.

The estimated average positioning errors of S-NPS, DFM-NU and H-FWM are compared in Table 2.

It can be found from Table 2 that the DFM-NU structure can significantly improve the precision of single foot-mounted module, while the H-FWM structure can simultaneously improve the precision of foot-mounted and waist-mounted positioning modules. Besides, the application of ultrasonic ranging significantly enhances the distance measurement ability for DFM-U structure, and further improve the positioning accuracy from the aspect of movement distance measurement. While the heading estimation error cannot be effectively eliminated using ultrasonic ranging approach, thus the magnetic observation applied in waist mounted module is also applied to provide heading calibration.

4.3. Evaluated results of H-PPS framework

Finally, the proposed H-PPS is evaluated under a comprehensive 3D indoor environment, and compared with state-of-art D-NPS algorithms to evaluate the accuracy improvement. In this case, the test route includes cross-floor indoor scene in Figs. 9 and 13, users

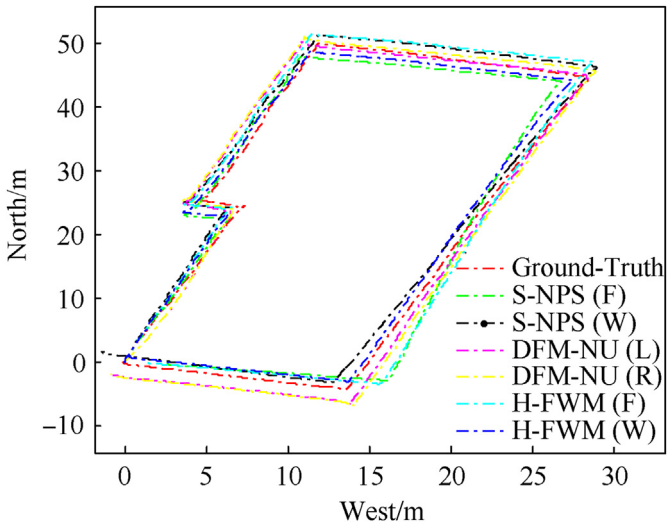

Fig. 11. Estimated trajectories by S-NPS, DFM-NU and H-FWM.

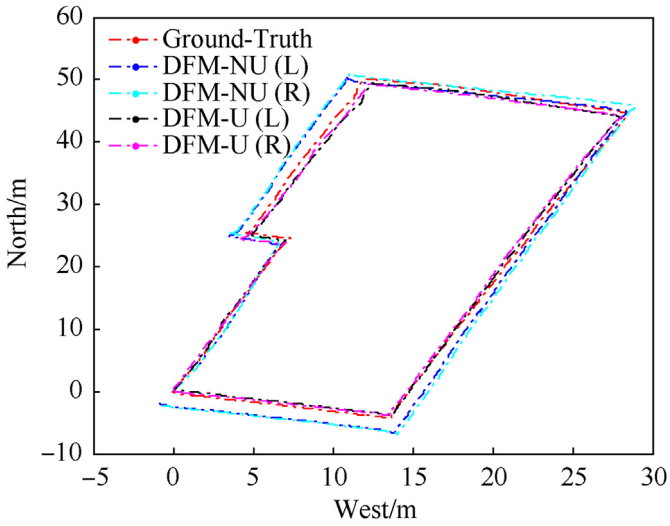

Fig. 12. Estimated trajectories by S-NPS, DFM-NU and H-FWM.

Table 2
Positioning errors comparison.

Structures	Average Error/m
S-NPS (F)	1.63
S-NPS (W)	1.32
DFM-NU (L)	1.26
DFM-NU (R)	1.19
H-FWM (F)	1.15
H-FWM (W)	1.04
DFM-U (L)	0.66
DFM-U (R)	0.59

started with the point A, walked through the point B-L, F, E, D, and back to the point A. The walking duration and walking distance are 294 m and 195 s, respectively.

This work proposed the DLSE to estimate the walking speed of the pedestrian using the integration of wearable inertial sensors and ultrasonic modules. To evaluate the performance of presented DLSE, the 1D-CNN [25], Bi-LSTM [17], and MLP [4] models are applied for comparison purposes under the same walking route and

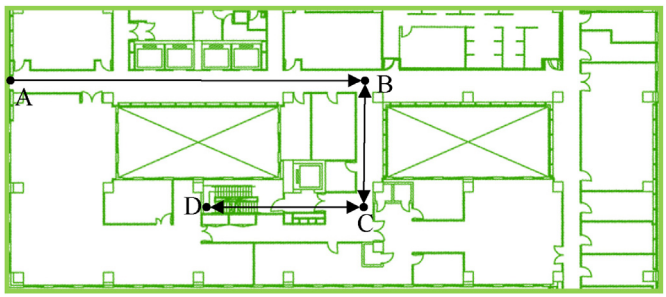

Fig. 13. Walking route in 10th floor.

training and testing datasets, the estimated speed estimation errors using different deep-learning models are compared as follows:

Table 3 indicates that the proposed DLSE model realizes the better speed estimation accuracy compared with three existing models including 1D-CNN, Bi-LSTM, and MLP, the estimated speed estimation error is lower than 0.052 in 75% cumulated percentage.

The positioning accuracy of overall proposed H-PPS is firstly compared with each subpart including DFM-U and S-NPS (W) under the same 2D route described in Fig. 10, the improved performance is described as follows:

It can be found from Table 4 that the presented H-PPS significantly enhances the performance of S-NPS and D-NPS by integrating features extracted from both modules, the combination of different sub-systems significantly improves the positioning accuracy of overall system.

In addition, a 3D environment is selected to comprehensively estimate the precision of developed H-PPS under a cross-floor indoor scene in Figs. 10 and 13. The estimated trajectories and related positioning errors provide by different subsystems originated from overall H-PPS structure are compared in Figs. 14 and 15.

Figs. 14 and 15 present that the meter-level positioning accuracy can be realized using the proposed H-PPS structure, the achieved accuracies of each sub-system reach 1.09 m (Right Foot), 1.06 m (Left Foot), and 1.29 m (Waist) in 75%, respectively.

Finally, the overall H-PPS framework is compared with the state-of-art D-NPS structures f^{2}IMU-R [19] and FPS-DU [17] under the same walking route, and the overall poisoning error is compared by considering each subsystem. The estimated positioning errors provide by three different structures under the same walking route are described as:

Table 3
Walking Speed Estimation Errors Comparison using Different Models.

Indexes/Models	DLSE	1D-CNN	Bi-LSTM	MLP
Mean/(m•s^{-1})	0.039	0.061	0.051	0.056
Std/(m•s^{-1})	0.025	0.049	0.029	0.031
Max/(m•s^{-1})	0.088	0.168	0.117	0.133
Min/(m•s^{-1})	0.005	0.012	0.016	0.031
75th/(m•s^{-1})	0.052	0.089	0.067	0.076
Median/(m•s^{-1})	0.029	0.046	0.036	0.041

Table 4
Positioning errors comparison of H-PPS.

Structures	Average Error	Improved Rate
S-NPS (W)	1.32 m (75%)	–
DFM-U (L)	0.66 m (75%)	–
DFM-U (R)	0.59 m (75%)	–
H-PPS (W)	0.71 m (75%)	46.2%
H-PPS (L)	0.45 m (75%)	31.8%
H-PPS (R)	0.42 m (75%)	28.8%

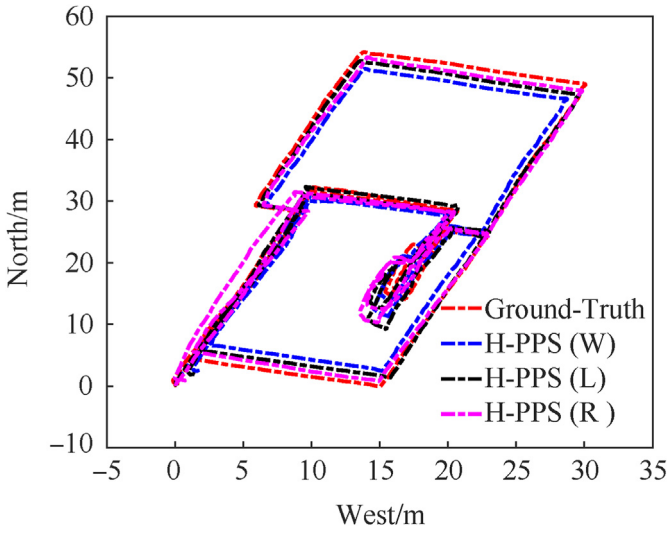

Fig. 14. Estimated trajectories for H-PPS.

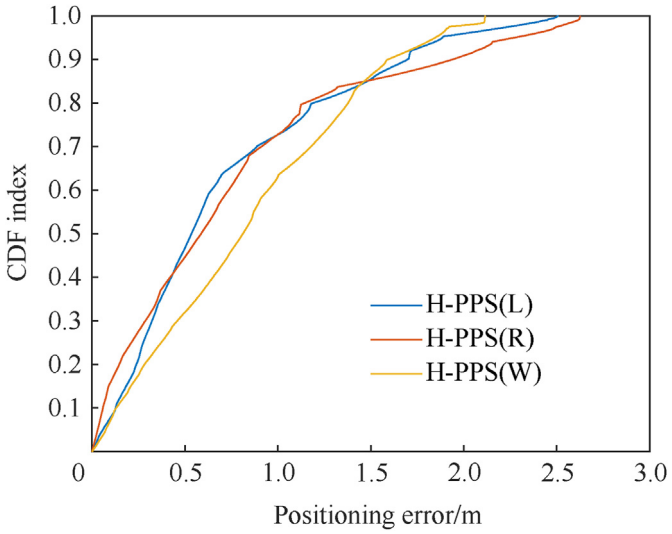

Fig. 15. Estimated positioning errors for H-PPS.

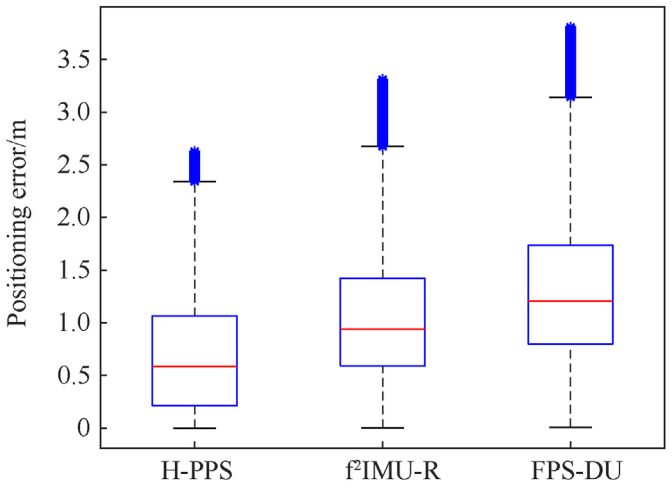

Fig. 16. Comparison results of different models.

Fig. 16 represents that the developed H-PPS proves better tracking performance compared with state-of-art algorithms, the estimated positioning errors under complex 3D environments reach 1.06 m in 75% (H-PPS), 1.42 m in 75% (f^2IMU-R), and 1.74 m in 75% (FPS-DU), respectively.

In summary, for S-NPS, the extracted multi-level constraints effectively enhance the performance of raw trajectory, and the waist-mounted positioning system realizes the higher accuracy (2.1 m in 75%) compared with the foot-mounted positioning system (3.78 m in 75%) under the same walking route and motion modes; For D-NPS, the experiments indicate that the combination foot-mounted and waist-mounted positioning modules can realize more accurate positioning accuracy (average 1.05 m) than the dual foot-mounted positioning system (average error 1.26 m), while the assistance of ultrasonic ranging can significantly enhance the performance of dual foot-mounted positioning system, achieves the meter-level positioning accuracy under test routes (average error 0.66 m); Finally, for the overall H-PPS, both S-NPS and D-NPS are integrated together, which effectively improve the positioning accuracies of S-NPS and D-NPS, respectively, and the best experimental results can reach the sub-meter level (0.42 m in 75%).

5. Conclusions

To increase the tracking performance of distributed IMU positioning system, this paper presents H-PPS, which can adaptively combine different single-mounted nodes including foot-mounted and waist-mounted nodes, and achieves much better combined positioning results compared with single node and state-of-art dual nodes structures. The experimental results indicate that the meter-level pedestrian tracking precision can be achieved using the integration of multiple IMU nodes and ultrasonic ranging results under complex 3D scenes.

Our future works will focus on more intelligent deep-learning network for pedestrian walking speed estimation and prediction, by extracting more comprehensive pedestrian motion features from different IMU nodes. In addition, more IMU nodes will be deployed in different parts of human body, for instance, thighs, arms, head et al., which can provide richer motion information of overall human body, more observations and constraints can be modeled to eliminate the cumulative error of single IMU node. Finally, the human motion is always complex and dynamic, which contains various motion modes for instance walking, jumping, running, backward walking, lateral walking, creep et al., and all of this motion modes need to be detected in real-time and considered as the comprehensive constraint factors in the H-PPS system.

Declaration of competing interest

The authors declare the following financial interests/personal relationships which may be considered as potential competing interests:

Acknowledgements

This work was supported by the National Natural Science Foundation of China under (Grant No. 52175531), and in part by the Science and Technology Research Program of Chongqing Municipal Education Commission under Grant (Grant Nos. KJQN202000605 and KJZD-M202000602).

References

[1] Liu L, Liu J, Qiu S, et al. Kinematics analysis of arms in synchronized canoeing with wearable inertial measurement unit. IEEE Sensor J 2023;23(5):4983–93.
[2] Wong MO, Zhou H, Ying H, et al. A voice-driven IMU-enabled BIM-based multi-user system for indoor navigation in fire emergencies. Autom ConStruct 2022;135:104137.
[3] Li C, Yu L, Fei S. Real-time 3D motion tracking and reconstruction system using camera and IMU sensors. IEEE Sensor J 2019;19(15):6460–6.
[4] Yu Y, Chen R, Chen L, et al. H-WPS: hybrid wireless positioning system using an enhanced wi-fi FTM/RSSI/MEMS sensors integration approach. IEEE Internet Things J 2021;9(14):11827–42.
[5] Sun X, Ai H, Tao J, et al. BERT-ADLOC: a secure crowdsourced indoor localization system based on BLE fingerprints. Appl Soft Comput 2021;104:107237.
[6] Barbieri L, Brambilla M, Trabattoni A, et al. UWB localization in a smart factory: augmentation methods and experimental assessment. IEEE Trans Instrum Meas 2021;70:1–18.
[7] Liu Z, Chen R, Ye F, et al. Precise, low-cost, and large-scale indoor positioning system based on audio dual-chirp signals. IEEE Trans Veh Technol 2022;72(1):1159–68.
[8] Chen L, Zhou X, Chen F, Yang L-L, Chen R. Carrier phase ranging for indoor positioning with 5G NR signals. IEEE Internet Things J Jul. 2022;9(13):10908–19.
[9] Yu Y, Zhang Y, Chen L, et al. Intelligent fusion structure for wi-fi/BLE/QR/MEMS sensor-based indoor localization. Rem Sens 2023;15(5):1202.
[10] Kuang J, Li T, Chen Q, et al. Consumer-grade inertial measurement units enhanced indoor magnetic field matching positioning scheme. IEEE Trans Instrum Meas 2022;72:1–14.
[11] Bao S, Shi W, Chen P, et al. A systematic mapping framework for backpack mobile mapping system in common monotonous environments. Measurement 2022;197:111243.
[12] Wan Q, Duan X, Yu Y, et al. Self-calibrated multi-floor localization based on wi-fi ranging/crowdsourced fingerprinting and low-cost sensors. Rem Sens 2022;14(21):5376.
[13] Zhang P, Li Y, Zhuang Y, et al. Multi-level information fusion with motion constraints: key to achieve high-precision gait analysis using low-cost inertial sensors. Inf Fusion 2023;89:603–18.
[14] Qin T, Li P, Shen S. Vins-mono: a robust and versatile monocular visual-inertial state estimator. IEEE Trans Robot 2018;34(4):1004–20.
[15] Mehrabian H, Ravanmehr R. Sensor fusion for indoor positioning system through improved RSSI and PDR methods. Future Generat Comput Syst 2023;138:254–69.
[16] Wu Y, Kuang J, Niu X. Wheel-INS2: multiple MEMS IMU-based dead reckoning system with different configurations for wheeled robots. IEEE Trans Intell Transport Syst 2022;24(3):3064–77.
[17] Qi L, Yu Y, Liu Y, et al. A robust foot-mounted positioning system based on dual IMU data and ultrasonic ranging. IEEE Sensor J 2023;23(4):4085–95.
[18] Niu X, Li Y, Kuang J, et al. Data fusion of dual foot-mounted IMU for pedestrian navigation. IEEE Sensor J 2019;19(12):4577–84.
[19] Zhu M, Wu Y, Luo S. f^2IMU-R: pedestrian navigation by low-cost foot-mounted dual IMUs and inter-foot ranging. IEEE Trans Control Syst Technol 2021;30(1):247–60.
[20] Yu N, Li Y, Ma X, et al. Comparison of pedestrian tracking methods based on foot-and waist-mounted inertial sensors and handheld smartphones. IEEE Sensor J 2019;19(18):8160–73.
[21] Qiu S, Zhao H, Jiang N, et al. Sensor network oriented human motion capture via wearable intelligent system. Int J Intell Syst 2022;37(2):1646–73.
[22] Niu X, Liu T, Kuang J, et al. Pedestrian trajectory estimation based on foot-mounted inertial navigation system for multistory buildings in postprocessing mode. IEEE Internet Things J 2021;9(9):6879–92.
[23] Shi W, Yu Y, Liu Z, et al. A deep-learning approach for modelling pedestrian movement uncertainty in large-scale indoor areas. Int J Appl Earth Obs Geoinf 2022;114:103065.
[24] Pham TT, Suh YS. Walking step length estimation using waist-mounted inertial sensors with known total walking distance. IEEE Access 2021;9:85476–87.
[25] Qi L, Yu Y, Liu Y, et al. Precise 3D foot-mounted indoor localization system using commercial sensors and map matching approach. Meas Sci Technol 2022;33(11):115117.